Soils and Rocks
An International Journal of Geotechnical and Geoenvironmental Engineering
www.soilsandrocks.com
ISSN 1980-9743
ISSN-e 2675-5475

Fiber reinforcement effectiveness in two different sand specimens

Murilo Pereira da Silva Conceição[1], Camilla Maria Torres Pinto[1], Miriam de Fátima Carvalho[1], Sandro Lemos Machado[1#]

Article

Keywords
FRS
Fiber-reinforced soils
Dilatancy
Grain size curve

Abstract

Fiber Reinforced Soils (FRS) are mixtures of discrete fibers with the soil to create a composite with improved mechanical properties compared to unreinforced material that depends on several soil and fiber properties. Therefore, comparative studies are needed to better understand their influence on FRS mechanical response. This paper analyzes the results of a comprehensive triaxial testing program performed on specimens of two different sands at the same relative density focusing on how the grain size distribution affects the composite behavior in terms of shear strength and dilatancy. It is shown that the grain size curve's uniformity coefficient (Cu) is one of the critical variables controlling FRS's dilatancy. Dune sand specimens (Cu = 1.79) presented dilatancy even for confining stresses as high as 300 kPa. The shear gains due to reinforcement were controlled by fiber length (L) and percentage (P_f), and size and shape of soil particles. River sand specimens with L = 51 mm and 1% fiber addition (dry mass) presented increments of 47.7 kPa in soil cohesion and a 5.2° increase in the soil friction angle compared to unreinforced material.

1. Introduction

The use of fiber Reinforced Soils (FRS) dates from ancient times. Vegetable fibers of jute and bamboo, among other species, were and are still used. However, Vidal (1966) conceived a soil reinforcement method using metallic strips recognized as the debut of the FRS modern use. FRS are mixtures of discrete fibers or strips with the soil to create a composite with improved mechanical properties compared to unreinforced material. The emergence of plastics offered newly manufactured durable fibers and reinforcement geosynthetics, such as geogrids, as an option to substitute metallic strips. FRS use can improve the mechanical behavior of soil in different applications, such as composing landfill cover layers, where their use could prevent superficial cracking due to wetting/drying cycles and differential waste mass settlements, which can lead to greenhouse gases emissions, embankments, earth dams, and other earthworks (Daniel & Benson, 1990; Daniel & Wu, 1993; Broderick & Daniel, 1990; Shackelford, 2014; Damasceno et al., 2019; Zhang et al., 2022).

Fiber length or aspect ratio (the relationship between the fiber length and its diameter/width), stiffness, fiber content, soil friction angle, and the coupled effects that occur in the soil grain/fiber interfaces are among the main parameters affecting the FRS mechanical behavior (Maher & Gray, 1990; Gao & Zhao, 2013; Michalowski, 2008; Li et al., 2020). Fiber orientation is also a critical factor interfering with the mechanical behavior of fiber-reinforced soils. Wang et al. (2017) present results of several triaxial tests with jute fibers disposed at different orientations. It is shown that vertical fibers had a negligible effect on composite shear strength. Horizontal fibers are most beneficial to the increase of peak deviator stress, with randomly oriented fibers also producing encouraging results. However, the laboratory moist tamping technique has presented a growing interest when using compacted specimens. This technique offers good control of specimen density, prevents fiber segregation, and produces a soil-fiber fabric that resembles that of FRS compacted in the field, although leading to the sub-horizontal orientation of fibers (Diambra et al., 2010).

Besides the early cited characteristics of fibers, some soil properties also play a paramount role in the overall FRS performance. Considering the universe of nonplastic coarse soils, the density index (I_D) is recognized as the main parameter controlling the mechanical behavior of coarse soils. Variations in friction angle between 6-10° are observed when coarse soils pass from a loose to a dense state (Leonards, 1962; Briaud, 2013). Furthermore, the grain size curve (GSC) parameters such as the coefficient of uniformity, typical grain size, and the roughness and shape of grains are also crucial variables that help understand solid/fiber interactions better.

#Corresponding author. E-mail address: smachado@ufba.br
[1]Universidade Federal da Bahia, Departamento de Ciência e Tecnologia dos Materiais, Salvador, BA, Brasil.

Submitted on November 27, 2022; Final Acceptance on March 19, 2023; Discussion open until August 31, 2023.
https://doi.org/10.28927/SR.2023.012422

The benefits associated with fiber reinforcement include but are not restricted to shear strength gains, higher ductility, smaller post-peak strength losses, and minored cracks appearance and propagation (Gray & Ohashi, 1983; Loehr et al., 2005; Choobbasti et al., 2019; Mandolini et al., 2019; Gao et al., 2020). Furthermore, fiber reinforcement is reported to increase the liquefaction and post-liquefaction shear strength of sand (Jain et al., 2023; Rasouli & Fatahi, 2022).

In this paper, compacted specimens from two different sands were submitted to a comprehensive triaxial testing program to evaluate the effects of fiber length, grain size curve parameters, and size, roughness, and shape of solid particles on the reinforcement effectiveness, measured in terms of the observed increments in the shear strength parameters, and FRS dilatancy.

2. Materials and methods

Table 1 summarizes the main characteristics of the employed sand, which were determined following the Brazilian standards ABNT NBR 6458 (ABNT, 2016a), ABNT NBR 7181 (ABNT, 2016b), ABNT NBR 12004 (ABNT, 1990), and ABNT NBR 12051 (ABNT, 1991). d_{xx} is the sieve equivalent diameter for a given percentage of the particles passing. *Cc* is the GSC curvature coefficient, and e_{max} and e_{min} are the maximum and minimum void ratios, respectively. *Gs* is the specific gravity of particles and ϕ_{pk} and ϕ_{ls} are the unreinforced soil friction angles for peak and large strain condition, respectively (approximating the friction angle at critical state conditions). As observed, dune sand presents a more uniform grain size curve and smaller particles. Additional details are provided in Conceição (2021) and Pinto (2021).

Table 1. Main characteristics of the employed sand.

Parameter	River sand	Dune sand
Particles' shape	Subangular	Rounded
d_{10} (mm)	0.43	0.176
d_{30} (mm)	0.59	0.25
d_{50} (mm)	0.83	0.29
d_{60} (mm)	0.96	0.315
Cu	2.24	1.79
Cc	0.84	1.13
G_s	2.65	2.657
e_{max}	0.79	0.748
e_{min}	0.52	0.523
ϕ_{pk} (º)	36.5	33.6
ϕ_{ls} (º)	32.8	30.5

Figure 1 illustrates the visual aspect of the river and dune solid particles. The larger size and less uniformity of the river sand grains than dune sand are easily noted, besides the subangular aspect of their particles.

FRS specimens used polypropylene fibers with lengths (*L*) of 12.5 mm, 25 mm, and 51 mm. As common properties, according to the manufacturer Viapol™, fiber diameter of $D = 0.51$ mm, specific gravity of $G_{sf} = 0.91$, fiber stiffness modulus of $E_f = 5.0$ GPa, and tensile strength of 500 MPa are cited. The adopted fiber contents (P_f, dry mass) were 0.5% and 1%. The experimental program considered fibers as part of the solid particles, calculating the composite's G_s value for each P_f. Figure 2 illustrates the visual aspect of the employed fibers. The specimen molding procedure used the moist tamping technique (Diambra et al., 2010).

Figure 3 illustrates the molding preparation steps. A vacuum pump provided an internal air pressure of about -15 kPa to preserve specimen integrity after mold removal. After molding, the specimen underwent vertical upward water flow until the permeability coefficient (*k*) stabilized. *k* values served as an indication of the molding process quality since small variations in molding conditions (especially in the void ratio) have a noticeable impact on *k*.

The experimental program used specimens with the same I_D (60%). Triaxial tests adopted the back pressure technique (Skempton's B parameter, $B > 0.95$) to saturate the specimens, which were then hydrostatically consolidated and

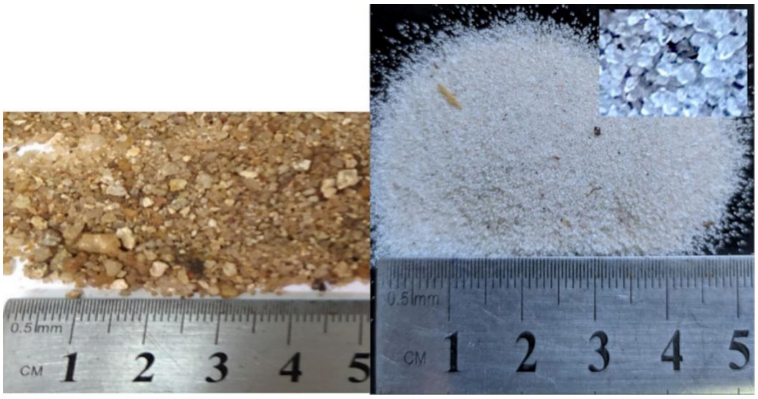

a) b)

Figure 1. Visual aspect of a) river sand and b) dune sand particles.

sheared under drained conditions (CD tests, Head & Epps, 2014). Tests imposed a displacement rate of 0.67 mm/min, and initial effective confining stresses of 50 kPa, 100 kPa, 200 kPa, and 300 kPa. Axial force, displacement, and volume changes were measured externally to the chamber. All the tests were performed in duplicate. Additional details can be found in Conceição (2021) and Pinto (2021).

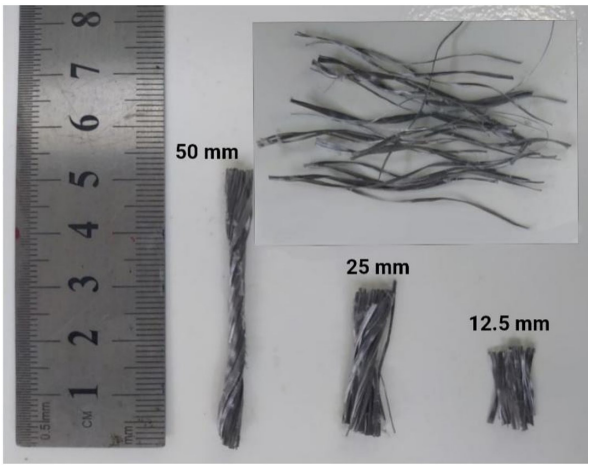

Figure 2. Visual aspects of employed reinforcement.

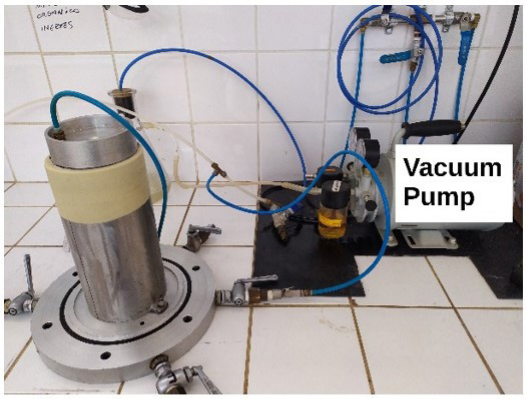

(a)

b)

Figure 3. a) end of the molding process and b) specimen aspect after mold removal (about -15 kPa air pressure applied by vacuum pump).

3. Results and analysis

Figures 4 and 5 illustrate some triaxial tests results in terms of deviator stress and volumetric strain curves for the performed tests. The presented results refer to tests performed with P_f = 0.5% and 1%, and confining stresses (σ_c) of 50 and 200 kPa. The results are coherent with many authors who cite the increase in composite cohesion, friction angle, and ductility, as well as the decrease in the after-peak shear strength reduction as fiber reinforcement effects (Ranjan et al., 1994; Diambra et al., 2010; Diambra et al., 2013; Gao & Diambra, 2021; Feuerharmel, 2000; Santiago, 2011; Michalowski & Čermák, 2003; Choobbasti et al., 2019; Li et al., 2020).

The fiber-reinforced sand specimens increased their shear strength with both fiber length and percentage, as reported by many other authors (Choobbasti et al., 2019; Li et al., 2020; Jishnu et al., 2020). Comparing pure soil and reinforced specimens with P_f = 1% and L = 51 mm, the composite shear strengths are approximately double that obtained for pure soil (see Figure 5). The cohesion was the most sensitive shear strength parameter to the fiber reinforcement, reaching values as high as 47.7 kPa for river sand specimens (see Table 2, P_f = 1% and L = 51 mm). For both sand, the fiber length was more effective in reinforcement than the fiber content since samples with P_f = 0.5% and L = 25 mm showed better resistance results than samples with P_f = 1% and L = 12.5 mm (Table 2). The observed behavior is the opposite of that reported by Fang et al. (2020), indicating that fiber-reinforcement effectiveness is dependent not only on P_f and L, but on a combination of fiber and soil characteristics.

Comparing the shear strength results of the two different sand composites, as expected, river sand specimens always presented higher peak and residual shear strength values. This results from its large and subangular particles and the less uniform grain size curve than dune sand.

As expected, specimens dilated more for lower confining stresses. However, dune sand specimens presented a dilation of about 2% even in the tests performed with σ_c = 200 kPa and higher, contrary to the river sand specimens. Different authors have reported a contradictory influence of fibers on composite dilation (Aguilar, 2015; Diambra et al., 2013; Festugato, 2008; Michalowski & Čermák, 2003; Rasouli & Fatahi, 2022).

Table 2 summarizes the shear strength parameters obtained considering all performed tests. For all the specimens, the failure criterion adopted was the maximum deviator stress. This corresponded to the peak stress in most cases, but in the cases of P_f = 1% and L = 51 mm specimens, the maximum strength occurred at 20% of axial deformation. As observed, the dune sand friction angle varied from 33.6º

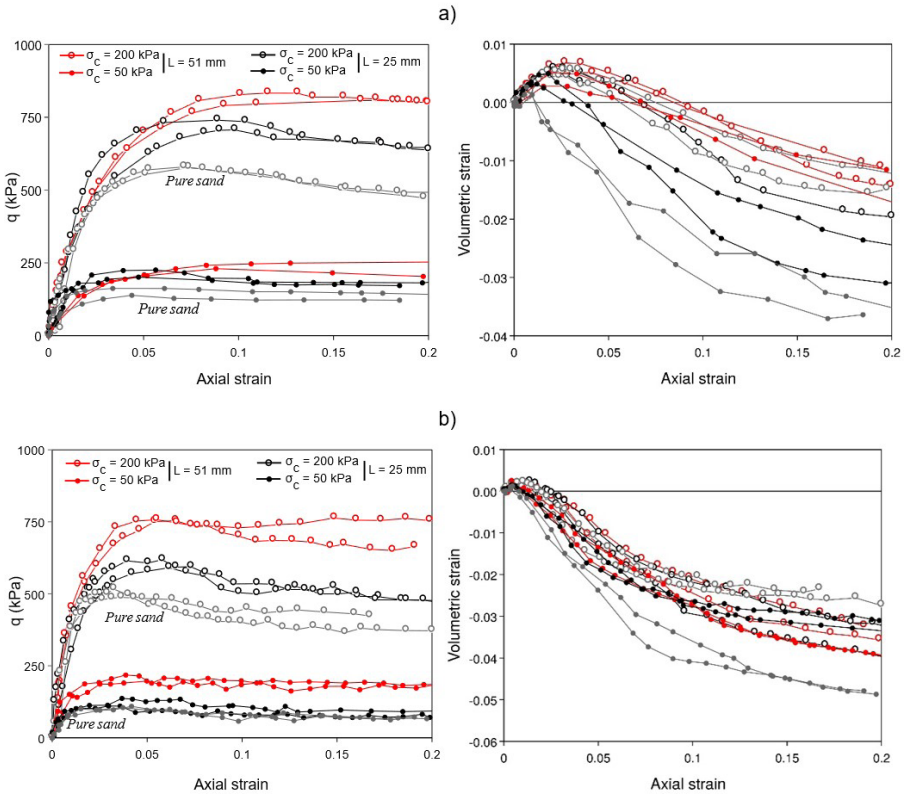

Figure 4. Deviator stress and volumetric strains versus axial strain curves. P_f = 0.5%, σ_c = 50 kPa and 200 kPa. a) river sand and b) dune sand specimens.

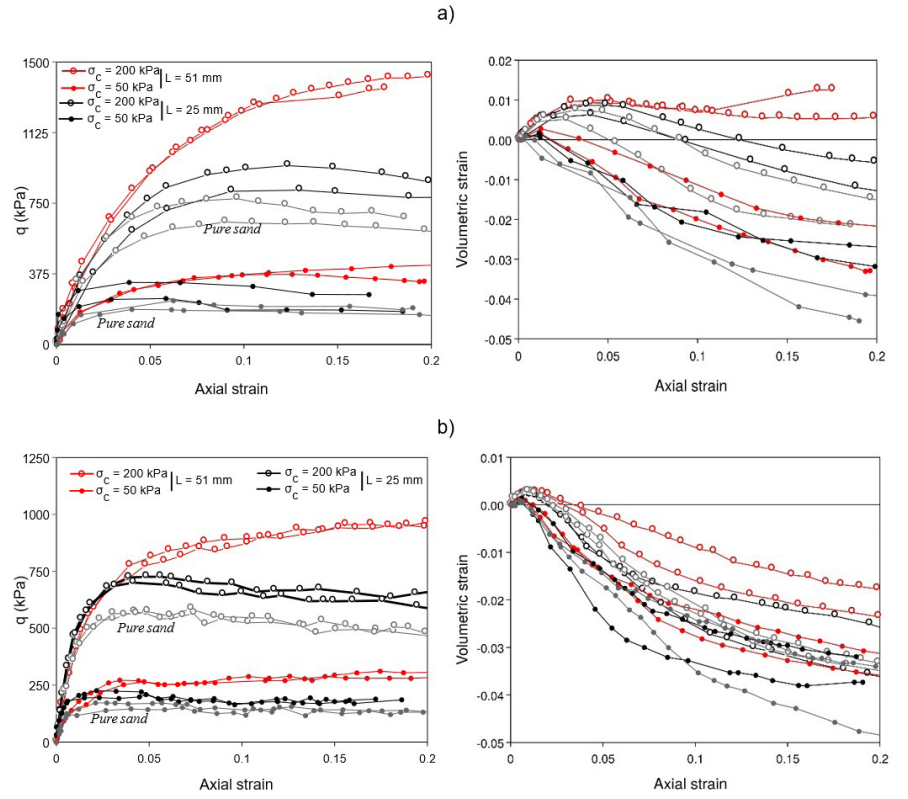

Figure 5. Deviator stress and volumetric strains versus axial strain curves. P_f = 1%, σ_c = 50 kPa and 200 kPa. a) river sand and b) dune sand specimens.

Table 2. Shear strength parameters for different fiber lengths and contents.

Material	Dune sand				River sand			
	c' (kPa)	ϕ' (º)	R^2 (-)	Δϕ′ (º)	*c'* (kPa)	ϕ' (º)	R^2 (-)	Δϕ′ (º)
Pure sand, P_f=0	0	33.6	0.9995	-	0	36.5	0.9998	-
P_f = 0.5%, L=25 mm	0	35.8	0.9994	2.2	9.5	39.2	0.9995	2.7
P_f = 0.5%, L=51 mm	7.2	40.7	0.9995	7.1	0	43	0.9993	7.4
P_f = 1%, L=12.5 mm	2.5	35.8	0.9995	2.2	8.2	39.2	0.9994	2.7
P_f =1%, L=25 mm	8.3	36	0.9995	2.4	19.6	41.7	0.9988	5.2
P_f =1%, L=51 mm	23.9	41.8	0.9987	8.2	47.7	41.7	0.9975	5.2

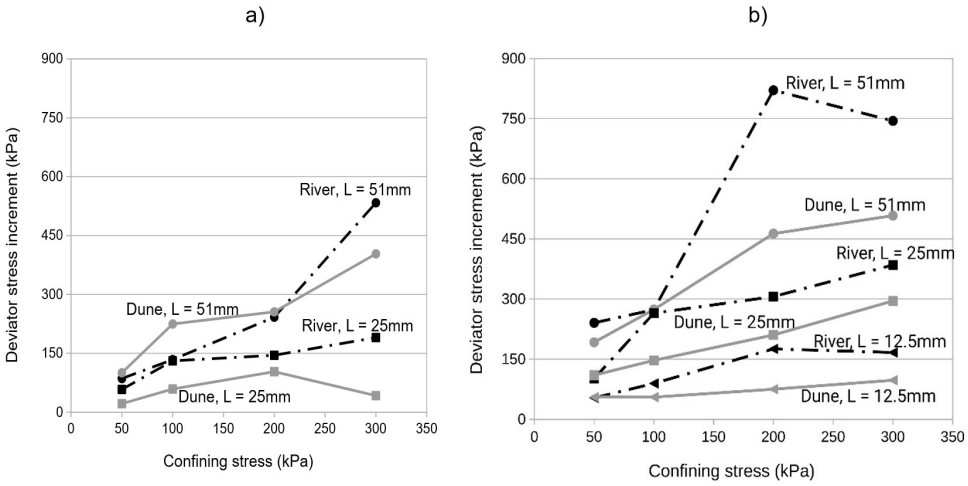

Figure 6. Fiber reinforcement effectiveness in terms of deviator stress increment. a) P_f = 0.5% and b) P_f = 1%.

to 41.8º and cohesion changed from 0 to 23.9 kPa from non-reinforced soil to composites with P_f = 1% and L = 51 mm. In contrast, variations from 36.5º to 41.7º and 0 to 47.7 kPa were observed for river sand specimens under the same conditions. Although a slightly smaller variation is kept in the friction angle of the river sand specimens, the cohesion increment was remarkably higher, and the final shear strength values of such composites are very promising.

Figure 6 presents the increments in q_{pk} as a function of P_f and σ_c. As observed, fiber reinforcement was more effective in the case of the river sand specimens. The authors believe the subangular shape and the larger size of the solid particles played an essential role in this case.

Figure 7 illustrates how the fiber length influences the stiffness and compressibility of the tested specimens. As observed (Figure 7a), increasing fiber length becomes samples more ductile in both cases (dune and river sands), and the peak stress occurs for higher axial strains, mainly in the case of fibers with L = 51 mm. However, volumetric behavior was much more complex and dependent on the grain size distribution. For lower confining stresses, the fiber tends to increase the soil dilatancy, no matter the soil tested in this study. For higher values of confining stress, river sand specimens, fibers become more effective in reducing dilatancy. However, this tendency is not observed in the case of the dune sand samples. The rounded shape and the smaller size of the dune specimens reduce the fiber reinforcement action not only in terms of shear strength but also when preventing soil volume increases. It also seems that the grain size curve uniformity prevails over particle size and shape, influencing the soil dilation since different authors (Michalowski & Čermák, 2003 and Ghadr et al., 2022) point to higher dilation in soils with coarser and angular grains.

Figure 8 illustrates how the mean dilatancy $(-\Delta\varepsilon_v/\Delta\varepsilon_a)$ before peak stress influences the soil shear strength in terms of the normalized difference between peak (q_{pk}) and large strain (q_{ls}) deviator stress. In this case, N_ϕ is given by Equation 1. As observed, river sand (RS) specimens presented an appreciable amount of tests with negative dilatancy (compression) or dilatancy values inferior to 0.1. This is coherent with the data shown in Figure 7b. Although data scattering, it is clear that dune sand specimens (DS) require higher dilatancy for the same gain in shear strength. However, for dilatancy values higher than 0.1, DS samples are more

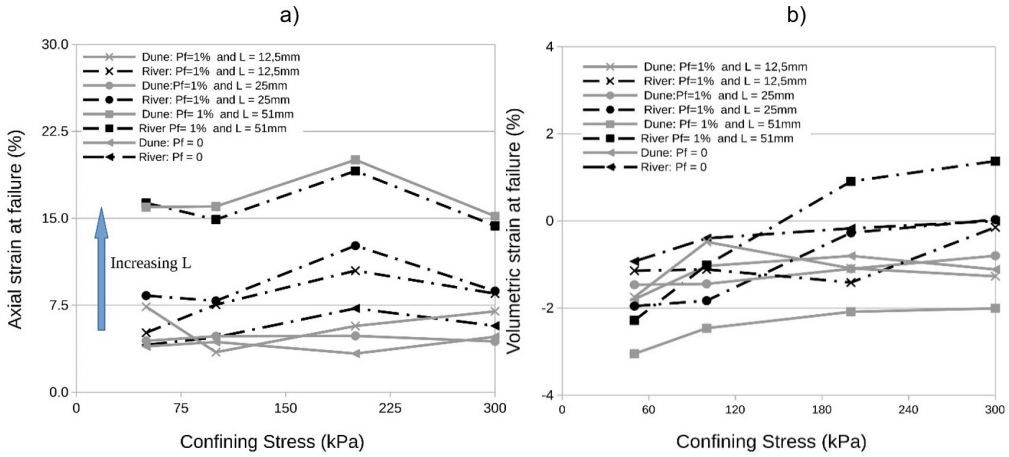

Figure 7. Effect of fiber length on axial and volumetric strains at failure for P_f = 1% specimens. a) axial strain behavior and b) volumetric strain behavior.

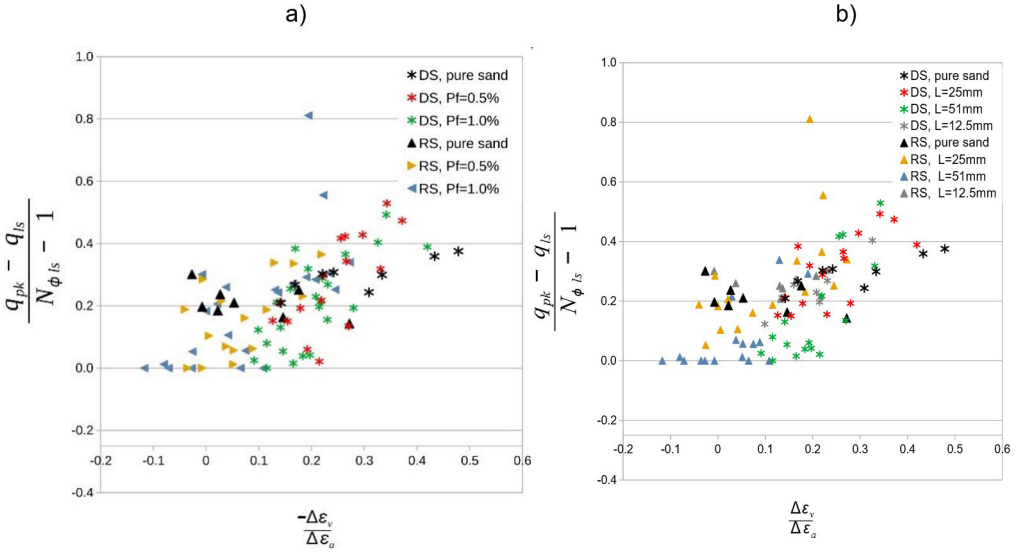

Figure 8. Dilatancy effect in increasing peak stress compared to residual values. a) comparing composites with different fiber percentage and b) comparing composites with fibers of different lengths.

responsive regarding shear strength gains due to dilatancy than RS specimens. In fact, only tests performed with L = 25mm (see Figure 8b) for RS specimens captured shear strength gains due to dilatancy. Non-reinforced and samples with L = 12.5 mm presented values of normalized deviator stress differences that are less sensitive to dilatancy in both soils. It is impossible to differentiate the behavior obtained for P_f = 0.5% and 1% (Figure 8a). The more ductile behavior of the reinforced samples with L = 51 mm (Figure 7a) reduced the dilatancy values presented in Figure 8b.

$$N_\phi = tan\left(\frac{90+\phi_{ls}}{2}\right)^2 \quad (1)$$

4. Conclusions

Although fiber-reinforced soils are an up-and-coming alternative in earthworks, their use requires a deep knowledge of the interactions between the solid particles and the reinforcement elements and how the properties of each phase interfere with the overall composite mechanical performance. This paper used the results of a comprehensive triaxial testing campaign performed in two different sand reinforced with the same type, length, and percentage of fibers. Samples differed mainly in grain shape and grain size curve characteristics, and tests employed composites with the same relative density. As expected, river sand specimens formed by subangular particles with less uniform grain size curves

than dune sand presented higher peak and residual shear strength values. Furthermore, more effective reinforcement effects were also observed for river sand specimens under the same testing conditions. Concerning the stiffness and volumetric behavior, fiber addition increased ductility in composites of both sand, which passed to present peak strength for higher axial values. At least for river sand specimens, composites tended to reduce dilation as the reinforcement increased. For dune sand specimens, this effect was much less noticeable. Composite dilatancy was much less pronounced in river dune specimens, mainly for higher P_f values. Dune sand specimens required higher dilatancy values for the same shear strength increments than river sand composites. However, dilatancy was more effective in increasing DS shear strength for dilatancy values higher than 0.1.

Acknowledgements

The authors would like to thank CAPES and FAPESB for supporting the research development and Viapol for supplying the polymeric fibers used in the tests.

Declaration of interest

The authors have no conflicts of interest to declare. All co-authors have observed and affirmed the contents of the paper and there is no financial interest to report.

Authors' contributions

Murilo Pereira da Silva Conceição: conceptualization, methodology, data curation, visualization. Camilla Maria Torres Pinto: conceptualization, methodology, data curation, visualization. Miriam de Fátima Carvalho: conceptualization, methodology, writing – review & editing. Sandro Lemos Machado: conceptualization, methodology, writing – original draft.

Data availability

The datasets generated analyzed in the course of the current study are available from the corresponding author upon request.

List of symbols

d_{xx}	Sieve's equivalent diameter for xx% of the particles passing
e_f	Void ratio at the end of the tests
e_{max}	maximum void ratio
e_{min}	Minimum void ratio
k	Permeability coefficient
q_{pk}	Deviator stress at peak stress
q_{ls}	Deviator stress at large strains (residual strength)
B	Skempton's B parameter
C_c	Curvature coefficient
Cu	Uniformity coefficient
D	Fibers' diameter
DS	Dune sand
E_f	Fiber stiffness modulus
FRS	Fiber-reinforced soil
G_s	Particles' specific gravity
GSC	Grain size curve
G_{sf}	Fiber's particles specific gravity
I_D	Density index
L	Lengths of the fibers
N_ϕ	Shear strength parameter
P_f	Fiber content (dry mass)
RS	River sand
ϵ_{af}	Axial strain at the end of the tests
ϵ_{vf}	Volumetric strains at the end of the tests
σ_c	Confining stress
ϕ_{ls}	Composite friction angle for large strain conditions
ϕ_{peak}	Composite friction angle for peak stress

References

ABNT NBR 12004. (1990). *Soil - Determination of the maximum index void ratio of cohesionless soils*. ABNT – Associação Brasileira de Normas Técnicas, Rio de Janeiro, RJ (in Portuguese).

ABNT NBR 12051. (1991). *Soil - Determination of minimum index void ratio of cohesionless soils - Method of test*. ABNT – Associação Brasileira de Normas Técnicas, Rio de Janeiro, RJ (in Portuguese).

ABNT NBR 6458. (2016a). *Gravel grains retained on the 4,8 mm mesh sieve - Determination of the bulk specific gravity, of the apparent specific gravity and of water absorption*. ABNT – Associação Brasileira de Normas Técnicas, Rio de Janeiro, RJ (in Portuguese).

ABNT NBR 7181. (2016b). *Solo: Análise Granulométrica*. ABNT – Associação Brasileira de Normas Técnicas, Rio de Janeiro, RJ (in Portuguese).

Aguilar, J.R.T. (2015). *Analysis of mechanical behavior of a sandy soil reinforced with coir fibers* [Master's dissertation, Pontifical Catholic University of Rio de Janeiro]. Pontifical Catholic University of Rio de Janeiro's repository (in Portuguese). https://doi.org/10.17771/PUCRio.acad.25737.

Briaud, J.L. (2013). *Geotechnical engineering: unsaturated and saturated soils*. Wiley.

Broderick, G.P., & Daniel, D.E. (1990). Stabilizing compacted clay against chemical attack. *Journal of Geotechnical Engineering*, 116(10), 1549-1567. http://dx.doi.org/10.1061/(ASCE)0733-9410(1990)116:10(1549).

Choobbasti, A.J., Kutanaei, S.S., & Ghadakpour, M. (2019). Shear behavior of fiber-reinforced sand composite. *Arabian Journal of Geosciences*, 12, 1-6. http://dx.doi.org/10.1007/s12517-019-4326-z.

Conceição, M.P.S. (2021). *Análise do comportamento tensão-deformação de um solo reforçado com fibra* [Master's dissertation]. Federal University of Bahia (in Portuguese).

Damasceno, L.A.G., Carvalho, M.F., & Machado, S.L. (2019). Methane fugitive emissions through the cover system of a MSW landfill cell. *Journal of Environmental Engineering and Science*, 14(3), 1-11. http://dx.doi.org/10.1680/jenes.19.00005.

Daniel, D.E., & Benson, C.H. (1990). Water content-density criteria for compacted soil liners. *Journal of Geotechnical Engineering*, 116(12), 1811-1830. http://dx.doi.org/10.1061/(ASCE)0733-9410(1990)116:12(1811).

Daniel, D.E., & Wu, Y.K. (1993). Compacted clay liners and covers for arid sites. *Journal of Geotechnical Engineering*, 119(2), 223-237. http://dx.doi.org/10.1061/(ASCE)0733-9410(1993)119:2(223).

Diambra, A., Ibraim, E., Russell, A.R., & Wood, D.M. (2013). Fibre reinforced sands: from experiments to modelling and beyond. *International Journal for Numerical and Analytical Methods in Geomechanics*, 37(15), 2427-2455. http://dx.doi.org/10.1002/nag.2142.

Diambra, A., Ibraim, E., Wood, D.M., & Russell, A.R. (2010). Fibre reinforced sands: experiments and modelling. *Geotextiles and Geomembranes*, 28(3), 238-250. http://dx.doi.org/10.1016/j.geotexmem.2009.09.010.

Fang, X., Yang, Y., Chen, Z., Liu, H., Xiao, Y., & Shen, C. (2020). Influence of fiber content and length on engineering properties of MICP-treated coral sand. *Geomicrobiology Journal*, 37(6), 582-594. http://dx.doi.org/10.1080/01490451.2020.1743392.

Festugato, L. (2008*). Análise do comportamento mecânico de um solo micro - reforçado com fibras de distintos índices de aspecto* [Master's dissertation, Federal University of Rio Grande do Sul]. Federal University of Rio Grande do Sul's repository (in Portuguese). Retrieved in November 27, 2022, from http://hdl.handle.net/10183/14740.

Feuerharmel, M.R. (2000*). Behaviour of soils reinforced with polypropylene fibres* [Master's dissertation, Federal University of Rio Grande do Sul]. Federal University of Rio Grande do Sul's repository (in Portuguese). Retrieved in November 27, 2022, from http://hdl.handle.net/10183/2804.

Gao, Z., & Diambra, A. (2021). A multiaxial constitutive model for fibre-reinforced sand. *Géotechnique*, 71(6), 548-560.

Gao, Z., & Zhao, J. (2013). Evaluation on failure of fiber-reinforced sand. *Journal of Geotechnical and Geoenvironmental Engineering*, 139(1), 95-106. http://dx.doi.org/10.1061/(ASCE)GT.1943-5606.0000737.

Gao, Z., Lu, D., & Huang, M. (2020). Effective skeleton stress and void ratio for constitutive modeling of fiber-reinforced sand. *Acta Geotechnica*, 15, 2797-2811. http://dx.doi.org/10.1007/s11440-020-00986-w.

Ghadr, S., Chen, C., Liu, C., & Hung, C. (2022). Mechanical behavior of sands reinforced with shredded face masks. *Bulletin of Engineering Geology and the Environment*, 81, 1-21. http://dx.doi.org/10.1007/s10064-022-02810-z.

Gray, D.H., & Ohashi, H. (1983). Mechanics of fiber reinforcement in sand. *Journal of Geotechnical Engineering*, 109(3), 335-353. http://dx.doi.org/10.1061/(ASCE)0733-9410(1983)109:3(335).

Head, K.H., & Epps, R.J. (2014). *Manual of soil laboratory testing: effective stress tests* (Vol. III). Whittles Publishing.

Jain, A., Mittal, S., & Shukla, S.K. (2023). Use of polyethylene terephthalate fibres for mitigating the liquefaction-induced failures. *Geotextiles and Geomembranes*, 51(1), 245-258. http://dx.doi.org/10.1016/j.geotexmem.2022.11.002.

Jishnu, V.P., Sankar, N., & Chandrakaran, S. (2020). Strength behaviour of cohesionless soil reinforced with coconut leaf let as a natural material. *Materials Today: Proceedings*, 31, S340-S347. http://dx.doi.org/10.1016/j.matpr.2020.04.637.

Leonards, G.A. (1962). *Foundation engineering*. McGraw Hill.

Li, L., Zang, T., Xiao, H., Feng, W., & Liu, Y. (2020). Experimental study of polypropylene fibre-reinforced clay soil mixed with municipal solid waste incineration bottom ash. *European Journal of Environmental and Civil Engineering*. In press. http://dx.doi.org/10.1080/19648189.2020.1795726.

Loehr, J.E., Romero, R.J., & Ang, E.C. (2005). Development of a strain-based model to predict strength of geosynthetic fiber-reinforced soil. In *Proceedings of Geo-Frontiers Congress: Geosynthetics Research and Development in Progress* (pp. 1-7). Austin: ASCE. http://dx.doi.org/10.1061/40782(161)20.

Maher, M.H., & Gray, D.H. (1990). Static response of sands reinforced with randomly distributed fibers. *Journal of Geotechnical Engineering*, 16(11), 1661-1677. http://dx.doi.org/10.1061/(ASCE)0733-9410(1990)116:11(1661).

Mandolini, A., Diambra, A., & Ibraim, E. (2019). Strength anisotropy of fibre-reinforced sands under multiaxial loading. *Geotechnique*, 69(3), 203-216. http://dx.doi.org/10.1680/jgeot.17.P.102.

Michalowski, R.L. (2008). Limit analysis with anisotropic fibre-reinforced soil. *Geotechnique*, 58(6), 489-501. http://dx.doi.org/10.1680/geot.2007.00055.

Michalowski, R.L., & Čermák, J. (2003). Triaxial compression of sand reinforced with fibers. *Journal of Geotechnical and Geoenvironmental Engineering*, 129(2), 125-136. http://dx.doi.org/10.1061/(ASCE)1090-0241(2003)129:2(125).

Pinto, C.M.T. (2021). *Estudo do comportamento mecânico de uma areia aluvionar reforçada com fibras* [Master's dissertation]. Federal University of Bahia (in Portuguese).

Ranjan, G., Vasan, R.M., & Charan, H.D. (1994). Behaviour of plastic-fibre-reinforced sand. *Geotextiles and Geomembranes*, 13(8), 555-565. http://dx.doi.org/10.1016/0266-1144(94)90019-1.

Rasouli, H., & Fatahi, B. (2022). Liquefaction and post-liquefaction resistance of sand reinforced with recycled

geofibre. *Geotextiles and Geomembranes*, 50(1), 69-81. http://dx.doi.org/10.1016/j.geotexmem.2021.09.002.

Santiago, G.A. (2011*). Estudo do comportamento mecânico de compósitos solo-fibras vegetais impermeabilizadas com solução de poliestireno expandido (EPS) e cimento asfáltico de petróleo (CAP)* [Doctoral thesis, Federal University of Ouro Preto]. Federal University of Ouro Preto's repository (in Portuguese). Retrieved in November 27, 2022, from http://www.repositorio.ufop.br/jspui/handle/123456789/3601.

Shackelford, C.D. (2014). The ISSMGE kerry rowe lecture: the role of diffusion in environmental geotechnics. *Canadian Geotechnical Journal*, 51(11), 1219-1242. http://dx.doi.org/10.1139/cgj-2013-0277.

Vidal, H. (1966). La terre Armée. *Annales de l'Institut Technique de Batiment et de Travaux Publics*, 58(259-260), 1-59. (in French)

Wang, Y, Guo, P., Ren, W. Yuan, B., Yuan, H., Zhao, Y., Shan, S., & Cao, P. (2017). Laboratory investigation on strength characteristics of expansive soil treated with jute fiber reinforcement. *International Journal of Geomechanics*, 17(11), 04017101. https://doi.org/10.1061/(ASCE)GM.1943-5622.0000998.

Zhang, J.Q., Wang, X., Yin, Z.Y., & Yang, N. (2022). Static and dynamic behaviors of granular soil reinforced by disposable face-mask chips. *Journal of Cleaner Production*, 331, 129838. http://dx.doi.org/10.1016/j.jclepro.2021.129838.